

## Comparing the physicochemical properties of printed and hand-cast biocements designed for ligament replacement

*Nazia Mehrban<sup>1</sup>, Jennifer Z. Paxton<sup>1</sup>, James Bowen<sup>1</sup>, Aminat Bolarinwa<sup>1</sup>, Elke Vorndran<sup>2</sup>, Uwe Gbureck<sup>2</sup> and Liam M. Grover\*<sup>1</sup>*

<sup>1</sup>School of Chemical Engineering, University of Birmingham, Birmingham, U.K.

<sup>2</sup>Department for Functional Materials in Medicine and Dentistry, University of Wurzburg, Wurzburg, Germany.

\*Corresponding author:

E-mail: [l.m.grover@bham.ac.uk](mailto:l.m.grover@bham.ac.uk)

Tel: +44-121-414-3887

Fax: +44-121-414-5324

### Abstract

In order to combat the low regenerative capabilities of ligaments full 'bone to bone' replacements are required, which will integrate with bone while providing a smooth transition to the replacement soft tissue (tissues surrounding organs in the body, not being bone). This study investigated the use of 3D powder printing technology to form calcium phosphate brackets, previously used for forming bespoke scaffold geometries, to  $95\% \pm 0.1\%$  accuracy of their original CAD design. The surface and internal structure of the printed samples was characterised both chemically and morphologically and compared with hand-moulded cements in the dry state and after 3 days of immersion in phosphate buffered saline. X-Ray Diffraction (XRD), Raman spectroscopy and scanning electron microscopy (SEM) all showed the presence of brushite in the hand-moulded samples and brushite and monetite within the printed samples. Furthermore, the printed structures have a higher level of porosity in the dry state in comparison to the hand-moulded ( $36 \pm 2.2\%$  compared to  $24 \pm 0.74\%$ ) despite exhibiting a compressive strength of almost double the hand cast material. Although the compressive strength of the printed cements decreases after the 3-day immersion, there was no significant difference between the printed and hand-moulded cements under the same conditions. 3D powder printing technology has enabled the manufacture of bespoke calcium phosphate brackets with properties similar to those reported for hand-moulded cements.

**Keywords:** Brushite, Monetite, 3D powder printing, calcium phosphate, tissue engineering, ligament

## Introduction

Tendons and ligaments are responsible for the attachment of bones to muscle or bone, respectively. Tendons function by transmitting forces between tissues with contrasting elastic moduli to facilitate movement, whereas ligaments act to stabilise joints. Approximately 800,000 tendon and ligament ruptures or tears occur every year in the USA., and are especially prevalent in young and active individuals.<sup>1</sup> Native ligaments and tendons have a low capacity to heal as a result of the low mitotic activity of the cell population within the tissue. As a consequence, surgical intervention is often required and the most common forms of reconstruction use the patient's own tissue which may be harvested from the patellar tendon or the distal semitendinosus tendon (hamstring). The success of the reconstruction can be limited by poor soft tissue adhesion to underlying bone, which means that the repair cannot withstand the mechanical demands of the rehabilitation regime. The principle cause of failure is the lack of the specialised interface found in intact ligaments or tendons, that prevent stress concentrations at the hard/soft tissue interface. Native tendons and ligaments can attach to bone via two different insertion types, a direct insertion and an indirect insertion. Indirect attachments are fibrous attachments in which the soft tissue attaches to the periosteum of hard tissue through extended collagen fibres known as Sharpey's fibres.<sup>2</sup>

Direct attachments are fibrocartilaginous and are separated into four distinct zones transitioning from the soft tendon or ligament tissue to the hard bone tissue. Both the presence of fibrocartilage and the gradual calcification that occurs within this region, act to dissipate stress at the insertion site.<sup>3</sup> Although both soft and hard tissue exhibit similar tensile properties,<sup>4</sup> it is the elastic modulus mismatch, where the elastic modulus of bone is ten times that of tendons<sup>3</sup> which is the primary reason direct surgical reattachment of tendons and ligaments to bone often fail.<sup>5</sup> Current methods of repair using synthetic materials include: sutures; fixation plates; silastic sheets; carbon fibres; and fibrin glues, however, a lack of a graded interface region induces common failure of these repair methods. Furthermore, the lack of graft availability, donor site morbidity, poor healing, graft failure requiring further surgery or a lifelong altered gait add to the disadvantages of current methods of tendon and ligament repair and alternative methods are required. One such method involves the formation of the hard/soft tissue constructs *in vitro*, which could subsequently be implanted to replace the function of the ligament or tendon.

It has previously been reported that it is possible to produce a ligament-like structure by culturing isolated tenocytes, tendon fibroblast cells, in a fibrin gel anchored to two calcium phosphate supports.<sup>6,7</sup> Since calcium phosphates are widely reported to form an intimate bond with both hard and soft tissues, the bond formed between the soft tissue and the ceramic was such that a passive tension caused collagen alignment between the brackets as is the case in native ligaments and tendons. More recently, it has been shown that by casting cement samples of different morphology for use in the system, it is possible to significantly improve tissue adhesion.<sup>8</sup> Recent studies have used rapid prototyping techniques to develop highly defined three-dimensional calcium phosphate structures for bone tissue regeneration.<sup>9,10</sup> The aim of this study was to characterise 3D calcium phosphate brackets engineered for the purpose of ensuring optimal adhesion between soft and hard tissue *in vitro*. The resulting samples were characterised with respect to their composition using Raman spectroscopy and X-ray diffraction while mechanical properties and microstructures were compared with samples formed using a standard hand-moulding method.

## Methodology

### *Production of 3D printed brackets*

Tricalcium phosphate (TCP) was synthesised by heating an equimolar mixture of dicalcium phosphate anhydrous (DCPA,  $\text{CaHPO}_4$ , monetite) (Merck, Darmstadt, Germany) and calcium carbonate (CC,  $\text{CaCO}_3$ , calcite) (Merck, Darmstadt, Germany) to a temperature of 1400°C for 14h followed by quenching at room temperature. The sintered cake was crushed with a pestle and mortar and passed through a 160  $\mu\text{m}$  sieve. Milling was performed in a planetary ball mill (PM400, Retsch, Germany) at 200 rpm with 500 mL agate jars, four agate balls with a diameter of 30 mm and a load of 125 g TCP per jar for 30 mins. Cement samples were printed with a multi-colour 3D-powder printing system (Spectrum ZS10, Z-Corporation, USA) using the TCP powder and a binder solution of 20% phosphoric acid (Merck, Darmstadt, Germany) with a layer thickness of 125  $\mu\text{m}$ , a binder/ volume ratio of 0.371 and an isotropic scaling  $x=y=z= 1.0$ . Structural geometries were designed using the thinkdesign 2007 software (Think3, Munich, Germany) to produce cylinders of height 12 mm and diameter 6 mm and discs of height 3mm and diameter 16mm. After printing, the loose powder on the samples was removed using compressed air and the exterior hardened by triplicate immersion in 20% phosphoric acid for 30 s.

### *Production of hand-moulded cements*

Hand-moulded brushite cements were made by combining  $\beta$ -TCP ( $\beta$ -tricalcium phosphate) with orthophosphoric acid (3.5 M + 200 mM citric acid + 200 mM sodium pyrophosphate) (Sigma-Aldrich, Gillingham, UK) at a powder to liquid ratio of 3.5 g/ml. The cement paste was consolidated into cylindrical PTFE moulds to give samples of height 12 mm and diameter 6 mm. Cement cylinders were left to set at 37°C overnight before being removed from the mould.

### *Compressive testing*

The compressive strength of the cement was determined by loading the cylindrical samples in parallel to their long axes at a constant cross head speed of 1 mm/min using a Universal testing machine (Z030, Zwick, Leominster, UK) equipped with a 30 kN load cell. For the immersed samples, the cements were first incubated in PBS for 3 days at 37°C prior to testing. After failure the fragments were collected and dried in ambient conditions prior to further characterisation.

### *Pycnometry*

The true density of the dried cement fragments was determined using a helium pycnometer (AccuPyc II 1340, Micromeritics, Dunstable, UK) with 10 purges prior to 10 measurements. Ten samples were measured for each condition, making the reported values an average of 100 measurements. The apparent density of the cement samples were calculated from geometrical measurements and the mass of the specimens. Relative porosity was then calculated using the values for apparent and true density. To evaluate ceramic microstructure, gold sputtered cement fracture surfaces were examined using scanning electron microscopy (Philips XL30 ESEM FEG, FEI, The Netherlands) at an accelerating voltage of 20kV.

### *X-ray diffraction*

The crystalline compositions of the cement samples were determined using X-ray diffraction. X-ray diffraction (XRD) patterns were recorded for printed and hand-moulded samples using a X-ray diffractometer equipped with an autosampler (D8, Bruker, Coventry, UK). Data were collected in the  $2\theta$  range 5° to 60° with a step size of 0.009 and a normalised count time of 1 s/step, using monochromatic  $\text{CuK}\alpha_1$  radiation from a Ge primary beam monochromator.

### *Raman spectroscopy*

Composition was also evaluated using a Raman microscope (WiTec Confocal Raman, LOT Oriel, UK). Raman spectral data for the cement samples were collected using a Peltier element cooled CCD detector in backscattering geometry and a grating set at 300 g/mm. High resolution scans with a spectral resolution of  $3\text{cm}^{-1}$  were obtained. For excitation, a 785nm solid state single frequency diode laser was used.

All data was presented as mean and standard error of the mean. Differences in mean values were compared within groups and significant differences were determined by ANOVA with a Tukey-Kramer HSD *post-hoc* test using BrightStat ([www.brightstat.com](http://www.brightstat.com)). The significance level was set at  $p < 0.05$ .

## Results

The 3D powder printing process was utilised to print several 3D structures for the attachment of calcium phosphates to soft tissue for creating bone to bone ligament replacements. CAD models were generated with morphologies optimised for retention of the soft tissue component (Fig. 1A) by creating re-entrant angles and also by providing a sandwich-like structure to maximise the surface area of the ceramic/soft tissue interface (Fig. 1B). The dimensions of the resulting brackets were 2 cm x 1.5 cm and by visual inspection, the printing process enabled the reproduction of bracket features with high accuracy (Fig. 1C and 1D). By comparing the dimensions of the CAD model with those of the printed parts, the accuracy of the process was quantified as  $95 \pm 0.1 \%$  (Table 1). As previous work on the tissue engineered hard/soft tissue interfaces focussed on using cements formed predominantly of brushite, further characterisations were undertaken to determine the influence of the printing process on the composition and mechanical properties exhibited by the hardened brackets.

The crystalline compositions of the cement samples were evaluated using XRD. The hand-moulded cements were shown to contain both unreacted  $\beta$ -TCP and brushite (Fig. 2A). While the printed samples contained both brushite and  $\beta$ -TCP, there were also peaks indicative of the formation of monetite within the hardened material (Fig. 2B). To further probe the composition of the materials regardless of crystallinity, samples were characterised using Raman spectroscopy.

From a comparison of the Raman spectra of the pre-moulded, 3D printed and reference materials, it was apparent that the chemical compositions of the ceramic monoliths were similar (Fig. 3). Peaks were present at  $413 \text{ cm}^{-1}$  and  $549 \text{ cm}^{-1}$  (P-O bending of the  $\text{PO}_4^{3-}$  ion),  $388 \text{ cm}^{-1}$  (O-H stretching) and a shoulder peak at  $892 \text{ cm}^{-1}$  represents the  $\text{HPO}_4^{2-}$  ion in the hydrated sample with a strong peak at  $985 \text{ cm}^{-1}$  shows P-O stretching from the  $\text{PO}_4^{3-}$  ion. Further P-O stretching modes are seen at  $1079\text{-}1166 \text{ cm}^{-1}$  ( $\nu_1$ ,  $\nu_2$ , and  $\nu_3$  respectively). Although the peaks present on the spectra collected from the ceramic materials were similar, in the case of the printed samples, the peaks indicative of the  $\text{HPO}_4$  in brushite were considerably more intense relative to the peaks characteristic of the  $\text{PO}_4$  vibration of  $\beta$ -TCP, indicating a greater degree of conversion from  $\beta$ -TCP to brushite or monetite.

Although there was a difference in the compositions of the bracket materials, the microstructures of the hardened materials were very similar. The outer surface of both structures consisted in the most part of long blade-like crystals (approximately  $20\mu\text{m}$  in length and  $2\text{-}5\mu\text{m}$  diameter), which is the morphology most frequently attributed to brushite (Fig. 4A and B).<sup>11</sup> The fracture surfaces of each material exhibited a similar microstructure, with the additional presence of irregularly shaped particles, most likely to be unreacted  $\beta$ -TCP (Fig. 4C and D).

The dry compressive strength of the printed cement samples was significantly higher ( $p < 0.05$ ) than the hand-moulded specimens ( $21.0 \pm 0.9$  compared with  $12.0 \pm 0.9$  MPa (Table 2), despite the fact that the porosity of the printed samples was significantly higher ( $p < 0.05$ ) than the hand-moulded specimens ( $36.0 \pm 2.2$  compared with  $24.0 \pm 0.7 \%$ ). In the case of both materials, immersion in PBS for a period of three days resulted in an increase of the porosity, 1% for the printed samples and 4% for the hand-moulded. Interestingly, the increase in porosity for the hand-moulded cement had no significant influence on compressive strength of the samples, however, immersion of the printed samples resulted in a significant reduction ( $p < 0.05$ ) of the strength of the cement from  $21.0 \pm 0.9$  to  $12.5 \pm 2.4$  MPa. This change in the compressive strength is not significantly different from the compressive strength of the hand-moulded cements under the same conditions ( $10.9 \pm 1.3$  MPa).

## Discussion

In this study a 3D powder printing process was used for the production of calcium phosphate brackets optimised for the attachment to soft tissues. The 3D printing process enabled the production of ceramics of complex morphology which would allow the soft tissue component of the scaffold to be sandwiched between two tessellating surfaces, maximising contact area and adhesion (Fig. 1). Previously, such structures have been fabricated using a cement casting method which limits the available geometries and requires a three-stage process.<sup>8</sup> The ceramic monoliths formed during this study were to within 95% accuracy of the original CAD models, as determined from geometrical measurements (Table 1).

The 3D printed specimens were compared with calcium phosphate structures formed using manual hand mixing, followed by casting to the required geometry. Despite the chemistries of the cement paste formed using each method being similar, X-ray diffraction (Fig. 2) and Raman spectroscopy (Fig. 3) showed that the compositions of the hardened materials were different. The structures formed using the cement casting method was formed of brushite and unreacted  $\beta$ -TCP, whereas those formed using 3D printing also contained a large proportion of monetite. The formation of monetite within the printed cement is more likely due to the dehydration of brushite formed initially within the matrix rather than the direct formation of monetite. This is because, although monetite is the more thermodynamically stable phase,<sup>12-14</sup> brushite crystal growth is an order of magnitude more rapid.<sup>15,16</sup> As such, monetite synthesis is not straightforward and typically requires the temperature of the reaction medium to be increased to  $>100^{\circ}\text{C}$ .<sup>17</sup> It has been demonstrated that dehydration can be caused by low local pH values,<sup>18</sup> temperature increase,<sup>19</sup> or extended storage in humid conditions.<sup>17</sup> The print head used for the deposition of the phosphoric acid onto the surface of the  $\beta$ -TCP had a resolution of  $118 \times 177$  dots per cm, and it is likely therefore that the ceramic surface was evenly covered by the orthophosphoric acid. In comparison with the cement paste, however, where the particles of  $\beta$ -TCP would have been evenly dispersed within the liquid phase, the acid was sprayed only onto the surface of the powder bed and thus could have resulted in a low localised pH value. The immersion of the hardened monoliths in the phosphoric acid may have further reduced the pH value to an extent that dehydration to monetite would have been likely. Indeed, it has previously been reported that the maintenance of a low pH within the cement matrix can cause dehydration in brushite cements.<sup>20</sup> Furthermore, the introduction of excess phosphoric acid in the hardening of the printed brackets, and not in the hand-moulded cements, increases monetite formation as demonstrated by Hofmann *et al.*<sup>21</sup> who showed that monetite formation increased when the citric acid concentration (also a setting retardant) was increased.

Although there was a compositional difference between the hardened materials, there was very little difference in the microstructures of the materials. Both ceramics consisted of blade-like crystals of approximately  $20 \mu\text{m}$  in length and  $2\text{-}5 \mu\text{m}$  in width (Fig. 4), consistent with the morphology of brushite and monetite as reported in the literature.<sup>22,23</sup> In the case of materials formed using both processes, the outer surface of the samples was shown to consist almost exclusively of blade-like crystals, whereas the centre of the samples consisted of some smaller irregularly shaped particles, which were most likely to be unreacted  $\beta$ -TCP (Fig. 4C and 4D). The reason for the heterogeneity of the samples could be the immersion in PBS prior to testing, which would have removed unbound  $\beta$ -TCP from the surface of the cement. Despite the microstructural similarity between the materials, the measured porosity differed significantly (by 12%, Table 2). The higher porosity exhibited by the printed samples could be attributed to the dehydration of the brushite phase to monetite. The density of brushite is  $2.32 \text{ g/cm}^3$  and monetite is  $2.89 \text{ g/cm}^3$ .<sup>20</sup> On dehydration of the brushite phase, therefore, a contraction of the matrix by 20% (for a fully reacted specimen) might be expected. Interestingly, however, despite the lower porosity of the hand-moulded cements, the strength exhibited by the 3D printed specimens was significantly higher prior to immersion. The most likely explanation for this is the higher degree of conversion from  $\beta$ -TCP of the printed cements as compared with the hand cast samples. On immersion in PBS, the strength of the 3D printed samples decreased by almost half, whereas there was no significant reduction in the strength of the hand cast samples (Table 2). One possible explanation for this could be the formation of monocalcium phosphate monohydrate within the samples, which can also form in low pH values.<sup>24</sup> The presence of such a phase prior to immersion and its subsequent dissolution may have caused the significant reduction in compressive strength. The presence of this phase in the amorphous state would have been extremely difficult to detect using XRD or Raman.

## **Conclusion**

In this study we have explored the suitability of powder printing technology for the design and development of geometrically complex 3D scaffolds for use in the engineering of tendon and ligament insertions. The printed structures were chemically and morphologically compared to hand-moulded samples. It was shown that samples can be produced by the 3-D printing process with 95% accuracy of the original CAD designs. Both hand-moulded and printed samples had similar crystal morphology, although monetite was shown to be also present in the printed cements. The porosity of the printed samples was found to be significantly higher than that of the hand-moulded samples with no difference to compressive strength between the two sample types after immersion in PBS. Future work will involve the assessment of cellular proliferation over time and the combination of printed samples with a soft tissue analogue for the potential use in tendon and ligament reconstruction.

**Acknowledgments**

The authors acknowledge the financial support of the BBSRC (Nazia Mehrban) and A.J. Wright for use of the X-ray diffractometer. The Helium pycnometer, Raman microscope and Universal testing machine used in this research were obtained, through Birmingham Science City: Innovative Uses for Advanced Materials in the Modern World (West Midlands Centre for Advanced Materials Project 2), with support from Advantage West Midlands (AWM) and part funded by the European Regional Development Fund (ERDF).

## References

1. D.M. Doroski , K.S. Brink and J.S. Temenoff: *Biomater*, 2007, **28**, 187-202.
2. M. Raspanti, C. Cesari and V. De Pasquale: *Arch Oral Biol*, 2000, **45**, 185–192.
3. M. Benjamin, H. Toumi, J.R. Ralphs, G. Bydder, T.M. Best and S. Milz: *J Anat*, 2006, **208**, 471–490.
4. S. Woo, J. Maynard and D. Butler: In 'Injury and Repair of the Musculoskeletal Soft Tissues' (eds Woo SL-Y, Buckwalter JA), 133–166; 1988, Park Ridge: Am Acad Orthop Surg.
5. R.B. Johnson: *Anat Rec a Discov Mol Cell Evol Biol*, 2005, **284A**, 485–490.
6. J.Z. Paxton, K. Donnelly, R.P. Keatch and K. Baar: *Tissue Eng Part A*, 2009, **15**, 1201-1209.
7. J.Z. Paxton, L.M. Grover and K. Baar: (2010a) *Tissue Eng Part A*, 2010a, In Press.
8. J.Z. Paxton, K. Donnelly, R.P. Keatch, K. Baar and L.M. Grover: *Annals Biomed Eng*, 2010b, **38**, 2155-2166.
9. U. Klammert, T. Reuther, C. Jahn, B. Kraski, A.C. Kübler and U. Gbureck: *Acta Biomater*, 2009, **5**, 727–734.
10. E. Vorndran, U. Klammert , M. Klarner, L.M. Grover, J.E. Barralet and U. Gbureck: *Dent Mater*, 2009, **25**, e18-e19.
11. M. Bohner, J. Lemaitre and T.A. Ring: *J Am Ceram Soc*, 1996, **79**, 1427-1434.
12. H.E. Lundage Madsen: *J Cryst Growth*, 1984, **66**, 369-376.
13. K.J. Lilley, U. Gbureck, J.C. Knowles, D.F. Farrar and J.E. Barralet: *J Mater Sc: Mater Med*, 2005, **16**, 455-460.
14. F. Tamimi-Mariño, J. Mastio, C. Rueda, L. Blanco and E. López-Cabarcos: *J Mater Sci: Mater Med*, 2007, **18**, 1195-1201.
15. M. Ohta and M. Tsutsumi: *J Cryst Growth*, 1982, **56**, 652-658.
16. S. Mandel and A. Cuneyt Tas: *Mater Sci Eng C*, 2010, **30**, 245-254.
17. J.G. Rabatin, R.H. Fale and A.E. Newkirk AE: *J Phys Chem*, 1960, **64**, pp. 491-493.
18. M.H. Prado Da Silva, J.H.C. Lima, G.A. Soares, C.N. Elias, M.C. de Andrade, S.M. Best and I.R. Gibson: *Surf and Coat Tech*, 2001, **137**, 270-276.
19. J.C. Elliot: In 'Structure and chemistry of the apatites and other calcium orthophosphates' 18; 1994, Elsevier Science B.V.: The Netherlands.
20. L.M. Grover, U. Gbureck, A.M. Young, A.J. Wright and J.E. Barralet: *J Mater Chem*, 2005a, **15**, 4955-4962.
21. M.P. Hofmann, A.M. Young, U. Gbureck and J.E. Barralet: *J Mat Chem*, 2006, **16**, 3199-3206.
22. J.E. Barralet, L.M. Grover and U. Gbureck: *Biomater*, 2004, **25**, 2197–2203.
23. A. Shkilnyy, J. Brandt, A. Manton, O. Paris, H. Schlaad and A. Taubert: *Chem Mater*, 2009, **21**, 1572–1578.
24. L.M. Grover, U. Gbureck, A.J. Wright and J.E. Barralet: *J Am Cem Soc*, 2005b, **88**, 3096–3103.

### Figure Legends

**Figure 1:** 3D brushite brackets printed on the powder printing system (Spectrum ZS10, Z-Corporation, USA). Images show the CAD model of a bracket (A) as well as the final printed structures (B) and the inner detail of these brackets (C and D).

**Figure 2:** X-ray diffraction pattern showing the phase composition of a hand-moulded cement (A) and a printed cement (B) with the printed sample containing some monetite in addition to brushite.

**Figure 3:** Raman spectra of hand-moulded (bold solid line) and printed cements (bold dashed line) with pure  $\beta$ -TCP (solid line) and pure brushite (dashed line). The spectra show vibrational frequencies of the different components in the cements.

**Figure 4:** SEM images showing the surface structure of printed samples (A), hand-moulded samples (B) and the fracture surface of printed samples (C) and hand-moulded samples (D).

### Table Legends

**Table 1:** Differences in the true density of non-immersed and immersed hand-moulded and printed samples and the printing accuracy of the printed cements.

**Table 2:** Differences in compressive strength and porosity of non-immersed and immersed hand-moulded and printed samples.

Figure 1

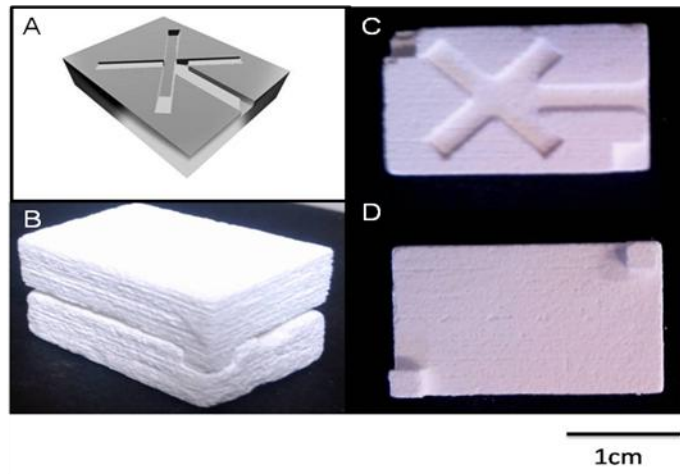


Figure 2

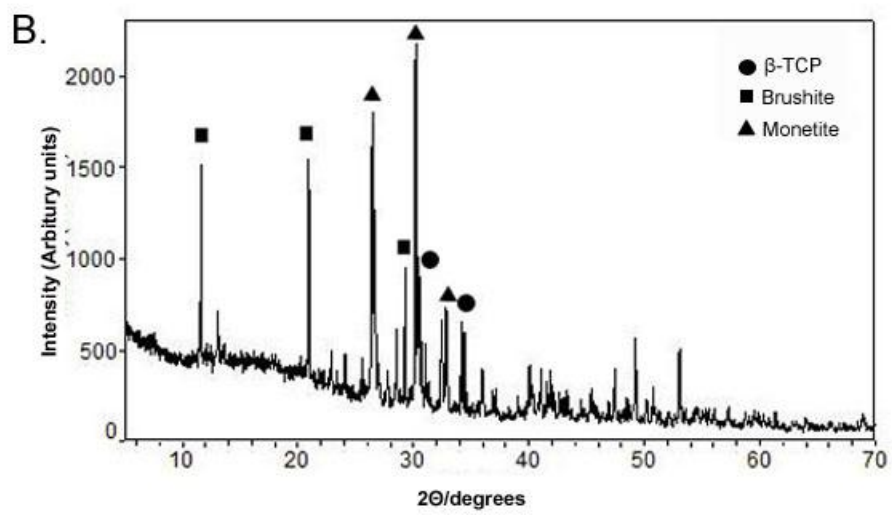
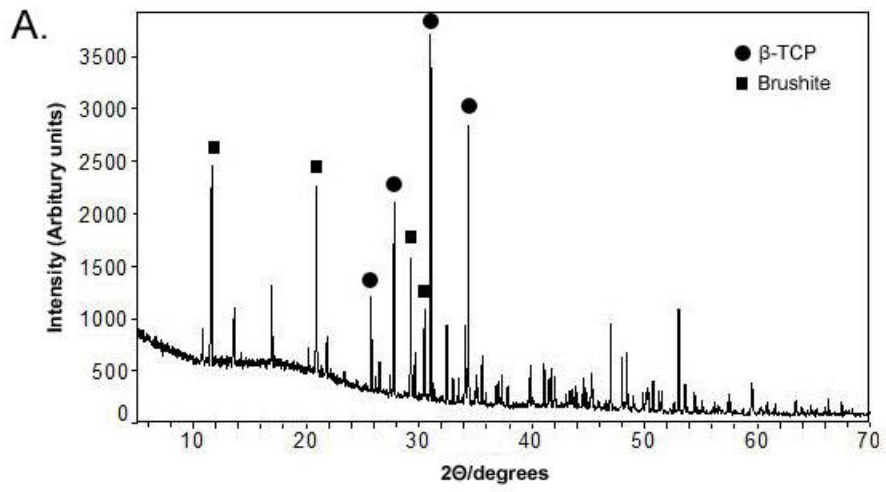


Figure 3

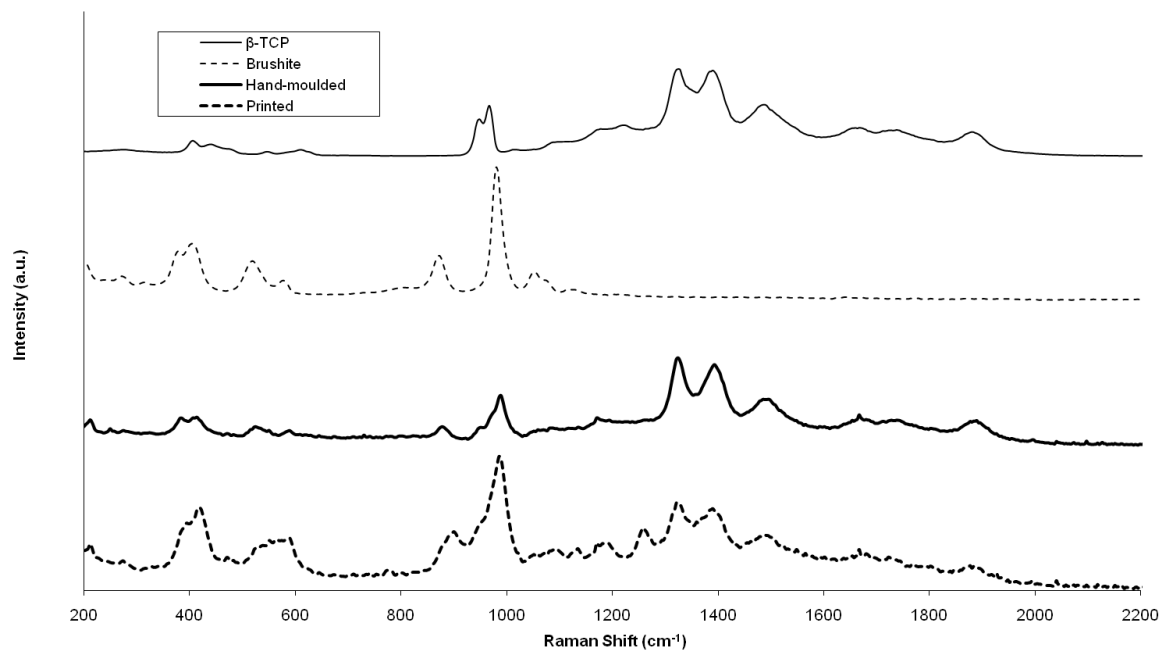


Figure 4

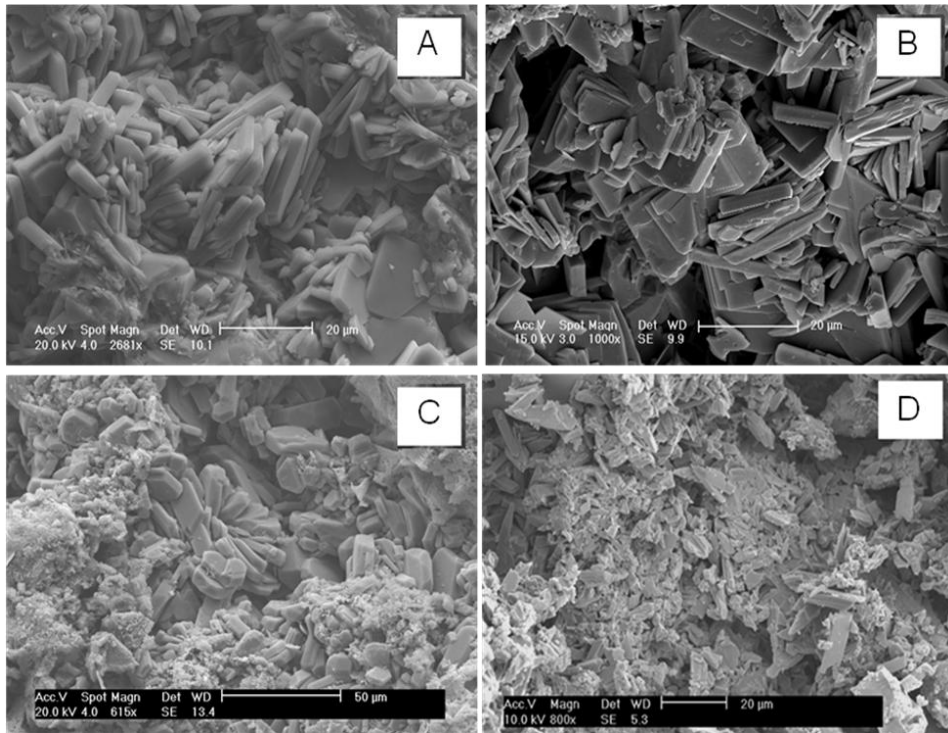


Table 1

	True density (gcm <sup>-3</sup> )		Printing Accuracy (%)
	Non-immersed	Immersed	
<b>Hand-moulded</b>	2.67 ± 0.01	2.72 ± 0.01	-
<b>Printed</b>	2.7 ± 0.02	2.65 ± 0.0	95 ± 0.1

\* denotes significantly different (p<0.05) to non-immersed samples of the same manufacturing process

# denotes significantly different (p<0.05) from hand-moulded samples of the same condition

Table 2

	Compressive strength (MPa)		Porosity (%)	
	Non-immersed	Immersed	Non-immersed	Immersed
<b>Hand-moulded</b>	12.04 ± 0.86	10.93 ± 1.34	24 ± 0.74	28 ± 1.32*
<b>Printed</b>	20.98 ± 0.9 #	12.49 ± 2.4*	36 ± 2.2 #	37 ± 1.35 #

\* denotes significantly different ( $p < 0.05$ ) to non-immersed samples of the same manufacturing process

# denotes significantly different ( $p < 0.05$ ) from hand-moulded samples of the same condition